Published OnlineFirst June 4, 2014; DOI: 10.1158/1535-7163.MCT-13-1063

FAK Inhibition Disrupts a β5 Integrin Signaling Axis Controlling Anchorage-Independent Ovarian Carcinoma Growth

Isabelle Tancioni, Sean Uryu, Florian J. Sulzmaier, Nina R. Shah, Christine Lawson, Nichol L.G. Miller, Christine Jean, Xiao Lei Chen, Kristy K. Ward, and David D. Schlaepfer

Abstract

Ovarian cancer ascites fluid contains matrix proteins that can impact tumor growth via integrin receptor binding. In human ovarian tumor tissue arrays, we find that activation of the cytoplasmic focal adhesion (FAK) tyrosine kinase parallels increased tumor stage, β5 integrin, and osteopontin matrix staining. Elevated osteopontin, β5 integrin, and FAK mRNA levels are associated with decreased serous ovarian cancer patient survival. FAK remains active within ovarian cancer cells grown as spheroids, and anchorage-independent growth analyses of seven ovarian carcinoma cell lines identified sensitive (HEY, OVCAR8) and resistant (SKOV3-IP, OVCAR10) cells to 0.1 μmol/L FAK inhibitor (VS-4718, formerly PND-1186) treatment. VS-4718 promoted HEY and OVCAR8 G_0–G_1 cell-cycle arrest followed by cell death, whereas growth of SKOV3-IP and OVCAR10 cells was resistant to 1.0 μmol/L VS-4718. In HEY cells, genetic or pharmacological FAK inhibition prevented tumor growth in mice with corresponding reductions in β5 integrin and osteopontin expression. β5 knockdown reduced HEY cell growth in soft agar, tumor growth in mice, and both FAK Y397 phosphorylation and osteopontin expression in spheroids. FAK inhibitor–resistant (SKOV3-IP, OVCAR10) cells exhibited anchorage-independent Akt S473 phosphorylation, and expression of membrane-targeted and active Akt in sensitive cells (HEY, OVCAR8) increased growth but did not create a FAK inhibitor–resistant phenotype. These results link osteopontin, β5 integrin, and FAK in promoting ovarian tumor progression. β5 integrin expression may serve as a biomarker for serous ovarian carcinoma cells that possess active FAK signaling. *Mol Cancer Ther; 13(8); 2050–61. ©2014 AACR.*

Introduction

Ovarian cancer is the fifth leading cause of cancer-related death in women in the United States (1). Initial tumor spread is by an exfoliative mechanism whereby cells dissociate from a primary site and can proliferate in an anchorage-independent manner as clumps of aggregated cells termed spheroids within the peritoneal space (2). Anchorage-independent growth is a hallmark of cell transformation and is connected to elevated tumorigenic potential (3).

In addition to being a sign of advanced disease, ascites contains growth factors and soluble matrix proteins that can enhance ovarian spheroid growth (4). Matrix proteins such as fibronectin, vitronectin, and osteopontin are ligands for integrin receptors and are present in high levels within ascites (5). Osteopontin is also a potential diagnostic blood biomarker for ovarian cancer (6, 7). Matrix proteins can become integrated within tumor spheroids to provide a structural scaffold as well as promote signals regulating tumor growth and survival (8, 9). Transmembrane integrin receptors bind matrix proteins and integrin α5β1 binding to fibronectin is linked to ovarian tumor metastasis in mouse models (10). However, clinical trials of an anti-α5β1 antibody did not show activity as a single agent in patients with platinum-resistant ovarian cancer (11). This may be due to signals from multiple β-integrin receptors for various matrix proteins that may require co-inhibition to prevent refractory ovarian tumor growth *in vivo*.

Integrin β integrin subunits activate a common set of cytoplasmic tyrosine kinases, and targeting this proximal linkage may be an effective means to block signals from multiple integrin receptors (12). The cytoplasmic focal adhesion (FAK) tyrosine kinase is recruited and activated by β1, β3, and β5 integrin subunits. These β integrins can pair with the αv integrin subunit, and together, signals are generated that modulate tumor survival and growth (13). FAK gene amplification occurs in about 24% of serous

Authors' Affiliation: Department of Reproductive Medicine, UCSD Moores Cancer Center, La Jolla, California

Note: Supplementary data for this article are available at Molecular Cancer Therapeutics Online (http://mct.aacrjournals.org/).

Corresponding Author: David D. Schlaepfer, Department of Reproductive Medicine, University of California San Diego, Moores Cancer Center, 0803, 3855 Health Sciences Dr., La Jolla, CA 92093. Phone: 858-822-3444; Fax: 858-822-7519; E-mail: dschlaepfer@ucsd.edu

doi: 10.1158/1535-7163.MCT-13-1063

Published OnlineFirst June 4, 2014; DOI: 10.1158/1535-7163.MCT-13-1063

ovarian cancer, and elevated FAK mRNA levels are associated with decreased overall patient survival (12). Although canonically known as a cell adhesion–activated kinase, FAK inhibition does not prevent the proliferation of tumor cells normally cultured on plastic (14, 15). However, increased tumor apoptosis occurs upon pharmacological FAK inhibition in mouse xenograft tumor models (16–18), and submicromolar concentrations can trigger apoptosis of tumor cell lines when cultured under anchorage-independent conditions (12, 19). Completed phase I trials of PF-00562271 FAK inhibitor revealed a subset of patients with stable disease (20), but molecular mechanisms driving tumor cell sensitivity or resistance to FAK inhibitors remain incomplete. Here, we show that FAK, β5 integrin, and osteopontin comprise a signaling axis promoting serous ovarian carcinoma tumor growth.

Materials and Methods

Antibodies and reagents

PND-1186 (ref. 21; renamed VS-4718 by Verastem Inc.) was from Poniard Inc. and PF-271 was synthesized as described (17). Compounds were dissolved in DMSO. Supplementary Table S1 contains antibody, plasmid, and probe sets used in this study. Additional materials and methods, including details of cell cycle, apoptosis, and real-time quantitative PCR analyses, are described in Supplementary Materials and Methods.

Cells

Supplementary Table S2 lists source, culture conditions, and selective DNA sequencing information for the cells used. Human ovarian cancer cell lines IGROV1, SKOV3, and SKOV3-IP were from J. Chien in 2008 (Mayo Clinic, Rochester, MN). OVCAR3, OVCAR8, and OVCAR10 cells were from D. Connolly in 2011 (cells generated at Fox Chase) and HEY cells were from S. Howell in 2011 (UCSD). BT474 cells were from ATCC (2008) and maintained in low passages (<3 months). For other cells, no authentication was performed by the authors. ID8-IP, IGROV1-IP, and SKOV3-IP cells were generated by intraperitoneal injection into nude mice in 2012 as described (12, 22). IGROV1, IGROV1-IP, SKOV3, SKVO3-IP, and HEY cells were cultured in DMEM; OVCAR3, OVCAR8, OVCAR10, and BT474 cells were culture in RPMI. All cell media were supplemented with 10% FBS, 0.1 nmol/L nonessential amino acids, 2 mmol/L glutamine, 100 U/mL penicillin, and 100 μg/mL streptomycin. Cell lines were propagated adherently on plastic and replated on low-binding poly 2-hydroxyethyl methacrylate (poly-HEMA, Corning)-coated plates for experimental anchorage-independent analyses.

DNA and retroviral constructs

shRNA targeting human FAK and a scrambled (Scr) control in pLentiLox 3.7-Puro were created as described (23). Lentiviral-transduced cells were selected by growth in puromycin; clones were isolated by single-cell sorting and characterized by anti-FAK immunoblotting. Three clones were pooled, expanded, and stored frozen as Scr- or FAK shRNA-expressing HEY cells. GFP-tagged FAK wild-type (WT) and FAK kinase-dead (KD) from the murine cDNA were cloned into the lentiviral vector pCDH1-MCS1-EF1-Puro (System Biosciences), selected for growth in puromycin, sorted via flow cytometry for GFP expression, and used as a pooled population. HEY cells were transduced with lentiviral shRNAs targeting human β5 integrin or Scr shRNA (Mission, Sigma). HEY and OVCAR8 cells were stably transduced with a myristoylated and membrane-targeted form of Akt (Addgene) via retrovirus produced by 293 cell transfection (23).

Cell growth

Cells were plated under adherent (0.5×10^4 cells, tissue culture–treated) and nonadherent conditions (25×10^4 cells, poly-HEMA–coated) in 6-well plates in 2 mL growth media. After 72 hours, all cells were collected by limited trypsin–EDTA treatment, a single-cell suspension was prepared, and the viable (trypan blue–negative) total cell number determined by ViCell XR counting (Beckman). For soft agar assays, 0.2×10^4 cells per well were plated in 0.3% agar in 0.2 mL growth media as described (12). After 7 days, colonies were stained with crystal violet, imaged in phase contrast, and enumerated. All experimental points were performed in triplicate and repeated at least 2 times.

Flow cytometry

For surface integrin expression, cells were trypsinized and incubated with primary antibodies to integrins (10^6 cells/μg antibody) for 60 minutes on ice and washed in cold PBS. Allophycocyanin (APC)-conjugated goat anti-mouse IgG was used as secondary antibody, and flow cytometry analyses (FACS Calibur) performed using FlowJo software. Mouse IgG was the negative control. For cell-cycle analyses, cells were collected as a single-cell suspension by limited trypsin treatment and fixed in 70% ethanol. Cells were incubated in 100 μL of PBS containing DNAse-free RNAse (100 μg/mL, Qiagen), and after 45 minutes, propidium iodide (PI; 5 μg/mL) was added before flow cytometry. For cell apoptosis analyses, cells were stained using APC-conjugated Annexin V and 7-amino-actinomycin (7-AAD; BD Pharmingen) and analyzed within 1 hour by flow cytometry.

Protein extracts and immunoblotting

Cell lysis buffer (1% Triton X100, 1% sodium deoxycholic acid, 0.1% SDS, 50 mmol/L HEPES, pH 7.4, 150 mmol/L NaCl, 10% glycerol, 1.5 mmol/L $MgCl_2$, 1 mmol/L EGTA, 10 mmol/L sodium pyrophosphate, 100 mmol/L NaF, 1 mmol/L sodium orthovanadate, 10 μg/mL leupeptin, 10 μg/mL aprotinin) was used to extract proteins from cultured cells and tumors as described (12). For conditioned media analyses, cells were cultured in serum-free OptiMEM (Life Technologies) for 24 hours, media collected, filtered (0.45 μm), and concentrated using centrifugal filtration (Millipore).

Published OnlineFirst June 4, 2014; DOI: 10.1158/1535-7163.MCT-13-1063

Immunohistochemistry

Paraffin-embedded normal ovarian and ovarian tumor tissue arrays were deparaffinized, rehydrated, processed for antigen retrieval, and peroxidase quenched as described (12). OV811, OV807, OV1502, and OV8010 (US Biomax) slides were used for β5 staining and OV811 used for FAK, pY397 FAK, and osteopontin. Tissues were blocked (PBS with 5% normal goat serum, 0.5% BSA, and 0.1% Triton X-100) for 45 minutes at room temperature (RT) and incubated with anti-pY397 FAK (1:100), anti-FAK (1:100), anti-β5 integrin (1:50), anti-osteopontin (1:500) in blocking buffer overnight. Biotinylated goat-anti-(rabbit/mouse) IgG or rabbit-anti-goat IgG (1:300), Vectastain ABC Elite, and diaminobenzidine were used to visualize antibody binding. Slides were counterstained with hematoxylin. Images were captured using an upright microscope (Olympus BX43) with color camera (Olympus SC100). Staining intensity scoring was blinded.

Frozen tumors were thin sectioned (7 μm) using a cryostat (Leica), mounted onto glass slides, fixed with acetone, permeabilized (PBS with 0.1% Triton) for 1 minute, and blocked (PBS with 8% goat serum) for 2 hours at RT. Sections were incubated in anti-αvβ5 integrin (1:200) in PBS with 2% goat serum overnight, washed, and incubated with goat-anti rabbit Alexa Fluor-647 with Hoechst 33342 to visualize nuclei. Images were acquired using a spinning disc confocal microscope (IX81; Olympus), OrcaER CCD camera (Hamamatsu), pseudo-colored, and merged using Adobe Photoshop.

Three-dimensional spheroid imaging

Tumor spheroid staining was performed as described (24), with some modifications. Spheroids were fixed and permeabilized for 3 hours at 4°C in PBS containing 4% PFA and 1% Triton X-100 with gentle rocking and then blocked in PBST (0.1% Triton X-100 in PBS) containing 3% BSA and 8% goat serum overnight at 4°C. Primary anti-pY397FAK (1:100) and anti-osteopontin (1:500) in PBST were incubated at 4°C for 24 hours followed by Alexa Fluor–conjugated secondary antibodies and Hoechst 33342 for 90 min at RT. Spheroids were mounted onto glass slides in 15 μL of PBS with 30 μL of Vectashield and images acquired using a Nikon Eclipse C1 confocal microscope (EZ-C1 3.50 imaging software).

Mouse tumor studies

Eight-week-old female nude (*nu/nu*) mice (UCSD breeding colony) were housed in pathogen-free conditions. Tumor cells were washed in PBS, injected (2×10^6 cells in 100 μL of PBS) subcutaneously into right and left flanks of nude mice, and tumor volume (length × width^2/2) determined by Vernier caliper measurements over 24 days. Orthotopic tumor growth was initiated by surgical implantation (0.4×10^6 cells in 7 μL of growth factor–depleted Matrigel) within the bursal region surrounding one ovary as described (12). Primary tumor weight was determined following euthanasia upon dissection. Fluorescent images of the intra-abdominal cavity and internal organs were acquired using an OV100 Small Animal Imaging System (Olympus). Blood was collected by heart puncture following euthanasia, samples were centrifuged, and serum was stored at −80°C. The UCSD Institutional Animal Care and Use Committee approved all mouse procedures.

Database analyses

The Kaplan–Meier plotter (25) was used to query gene expression and survival data from Gene Expression Omnibus and The Cancer Genome Atlas (Affymetrix HG-U133A, HG-U133A 2.0, HG-U133 Plus 2.0, and U95Av2 microarrays). Probes used are listed in Supplementary Table S1. Query parameters were overall survival, split patients by median, auto-select best cut-off, and follow-up threshold of 10 years. Restriction analyses were stage (all), histology (serous), grade (all), optimal debulk (all), and chemotherapy treatments (all). A total of 1,038 patient samples were analyzed and HRs and log-rank *P* significance were calculated via website interface.

Statistical analysis

Differences between groups were determined using one-way ANOVA with Tukey *post hoc* analyses (Prism). Differences between pairs of data were determined using an unpaired 2-tailed Student t test (Prism). Differences between β5 integrin in normal ovary, stage I, and stages II–IV was determined using the Kruskal–Wallis test. $P < 0.05$ was considered significant.

Results

Osteopontin, β5 integrin, and FAK levels correlate with serous ovarian cancer patient survival

Whereas integrins αv and β1 can promote ovarian carcinoma growth, elevated β3 integrin expression may inhibit tumor progression (26, 27). Although increased β5 integrin levels are part of an unfavorable ovarian cancer gene signature (28), limited IHC analyses detected αvβ5 reactivity only in ovarian tumors of low malignant potential (29). Therefore, connections between αvβ5 integrin and ovarian tumor progression remain unclear. We evaluated the importance of β5, αv, β3, and β1 integrin mRNA levels in a large annotated database of ovarian cancer patient samples (Fig. 1). Kaplan–Meier analyses showed that elevated β5, αv, and β1 integrin levels are significantly associated with decreased patient survival (Fig. 1A). In contrast, β3 integrin levels were not associated with patient survival differences (Fig. 1A). Expression of matrix ligands for αvβ5 integrins such as osteopontin and a downstream target of αvβ5 signaling such as FAK were also significantly associated with decreased patient survival (Fig. 1A).

Increased β5 integrin staining in stage II–IV serous ovarian tumors

As determined by tumor staining, increased FAK, pY397 FAK, and osteopontin levels correlate with a poor

Published OnlineFirst June 4, 2014; DOI: 10.1158/1535-7163.MCT-13-1063

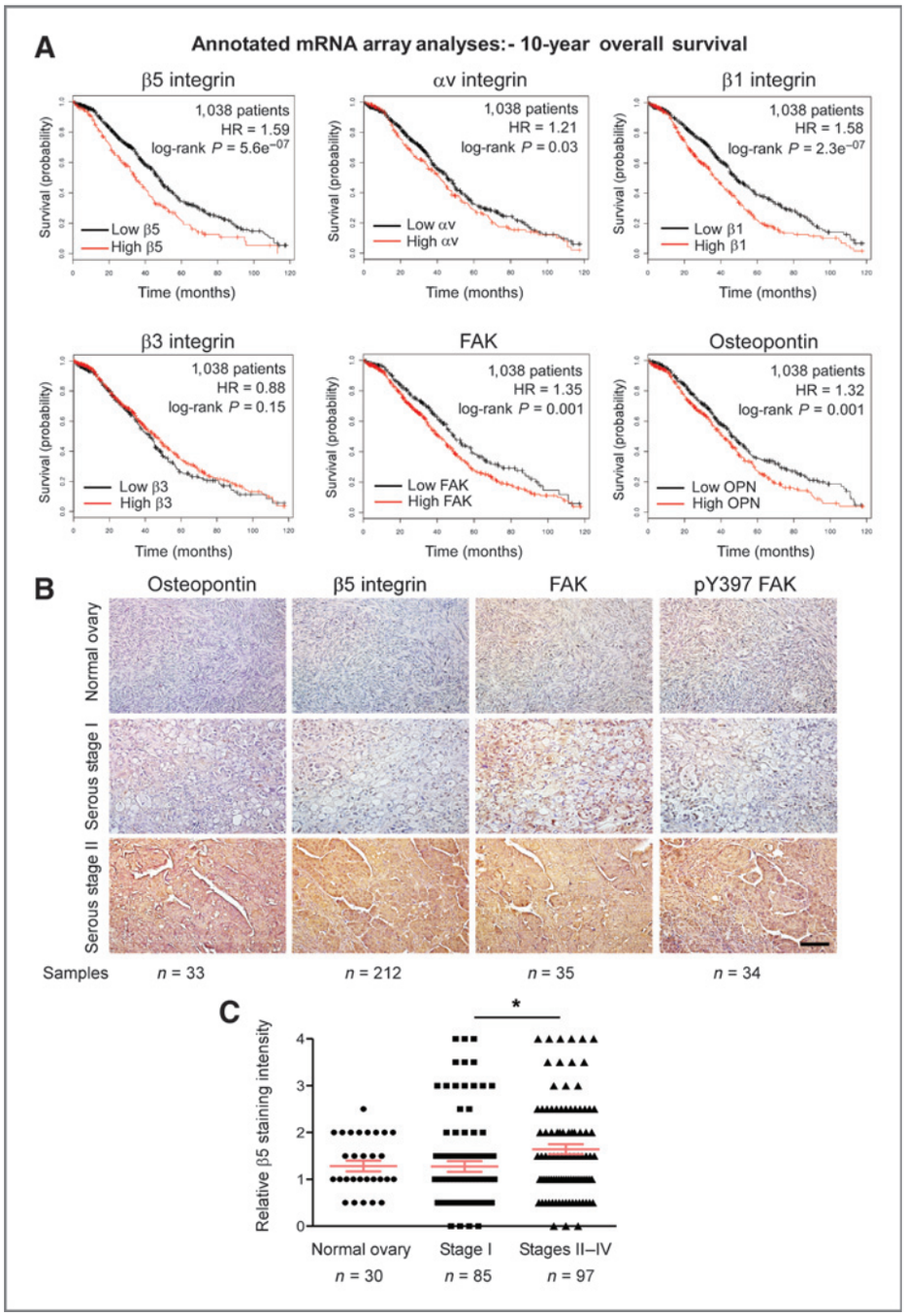

Figure 1. Association between osteopontin, β5 integrin, and FAK activation in serous ovarian cancer. A, Kaplan–Meier analyses of integrin β5, αv, β1, β3, FAK, and osteopontin (OPN) mRNA levels in 1,038 patient samples. High (red) versus low (black) mRNA expression shows patient overall survival probability over 120 months. HRs and log-rank *P* significance values are shown (inset). B, representative IHC staining of sections obtained from paraffin-embedded normal ovary, serous stage I, and serous stage II ovarian tumor tissue arrays using antibodies to pY397 FAK, total FAK, β5 integrin, and osteopontin. Scale, 100 μm. C, β5 integrin staining intensity (0–4) in annotated ovarian tissue arrays. Values are means (±SEM; *, $P < 0.05$, $n =$ sample number).

ovarian cancer patient prognosis (6, 30, 31). Staining of tumor tissue array serial sections with antibodies to osteopontin, FAK, FAK pY397, and β5 integrin revealed parallel increases as a function of tumor stage (Fig. 1B and Supplementary Fig. S1A). Specificity of FAK pY397 staining was confirmed by analyses of ID8-IP ovarian tumors from mice treated with vehicle or PF-271 FAK inhibitor (Supplementary Fig. S1B). Additional tumor tissue array staining analyses revealed no difference between β5 integrin levels in normal ovary tissue and stage I serous tumors (Fig. 1C). However, analyses of advanced stages II–IV tumors that present foci of dissemination showed significantly increased β5 integrin staining compared with stage I tumors that are confined to the ovary (Fig. 1C, $P < 0.05$). Together with the mRNA array analyses, these results support the hypothesis that osteopontin, αvβ5 integrin, and FAK activity may function as a signaling axis promoting ovarian tumor progression. Moreover, β5 integrin expression may serve as a biomarker for serous ovarian carcinoma cells that possess active FAK.

Published OnlineFirst June 4, 2014; DOI: 10.1158/1535-7163.MCT-13-1063

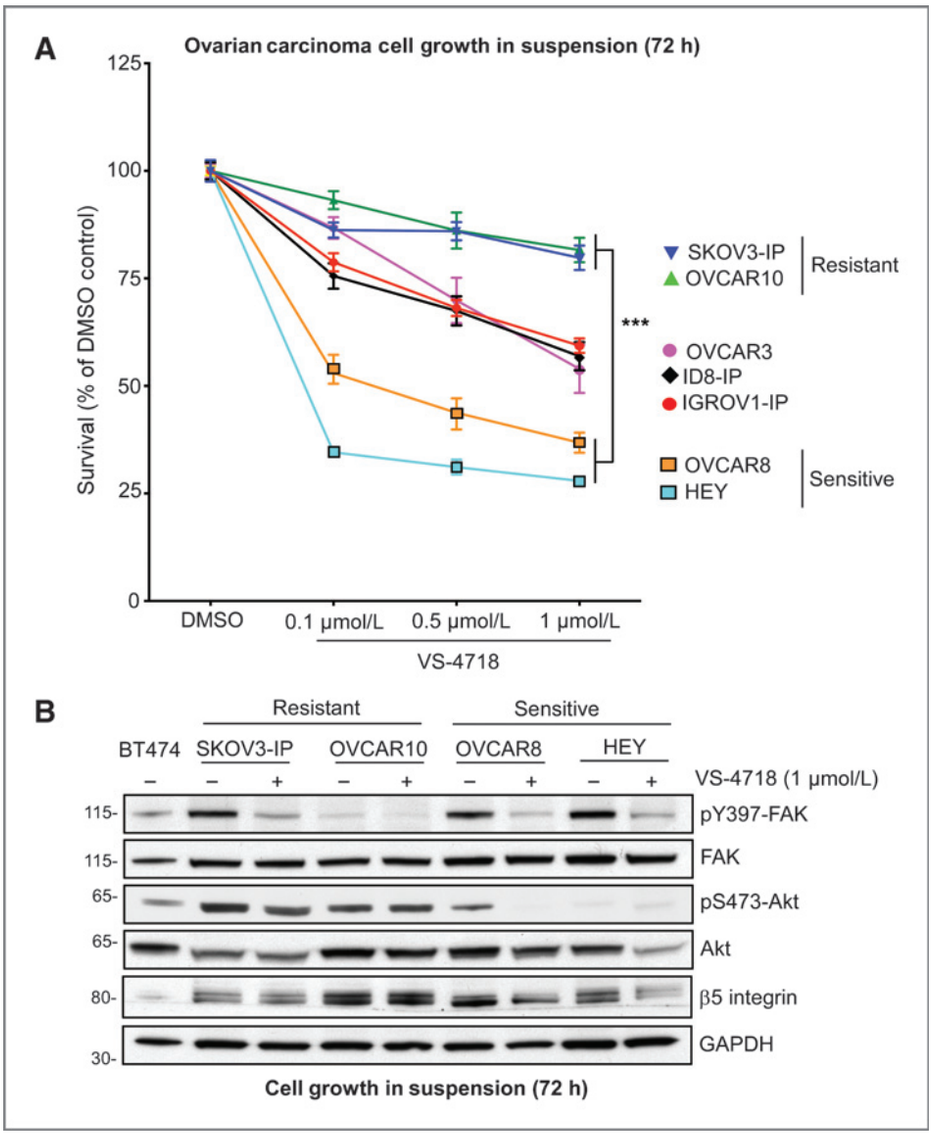

Figure 2. Identification of FAK inhibitor–sensitive and -resistant ovarian carcinoma cells. A, the indicated ovarian carcinoma cell lines were evaluated for anchorage-independent growth over 72 hours in DMSO (control) or increasing concentrations of VS-4718 (0.1–1.0 μmol/L). Values are means (±SEM) of triplicate points from 3 independent experiments (***, $P < 0.001$ vs. control). B, lysates of the indicated cells cultured in suspension with DMSO or VS-4718 (1 μmol/L) for 72 hours were analyzed by immunoblotting for pY397 FAK, pS473 Akt, and β5 integrin levels. Corresponding levels of total FAK, Akt, and GAPDH are shown. BT474 breast carcinoma cells are a positive control for pS473 Akt.

Identification of FAK inhibitor–sensitive and -resistant ovarian cancer cells

Analyses of seven ovarian carcinoma cell lines in anchorage-independent growth assays identified sensitive (HEY, OVCAR8) and resistant (SKOV3-IP, OVCAR10) cells to 0.1 μmol/L FAK inhibitor (VS-4718) addition (Fig. 2A). SKOV3-IP and OVCAR10 cells remained resistant with up to 1.0 μmol/L VS-4718 for 72 hours, whereas OVCAR3, ID8-IP, and IGROV1-IP cells exhibited an intermediate growth-inhibitory response. Flow cytometric analyses were performed to determine whether VS-4718 (1 μmol/L, 72 hours) triggered cell death (7-AAD staining and Annexin V binding) and/or alterations in cell-cycle progression in sensitive (HEY, OVCAR8) or resistant (SKOV3-IP, OVCAR10) cells. Early (Annexin V–positive) and late (Annexin V and 7-AAD–positive cells) OVCAR8 apoptotic cells were detected as well as OVCAR8 cells with G_0–G_1 block, and decreased S-phase cell-cycle percentage upon VS-4718 treatment (Supplementary Fig. S2). HEY cells did not exhibit changes in apoptosis, but VS-4718 blocked HEY cell-cycle progression (Supplementary Fig. S2). Treatment of OVCAR10- or SKOV3-IP–resistant cells with 1 μmol/L VS-4718 did not alter cell-cycle progression or promote cell death (Supplementary Fig. S2). Thus, in sensitive cells, FAK inhibitor treatment promotes G_0–G_1 cell-cycle arrest followed by cell death.

Previous studies implicated the PI3K/Akt kinase pathway as a downstream target of FAK in ovarian tumor cells (31, 32). Akt activation is common in high-grade, late-stage serous ovarian tumors (33). To gain insights into molecular targets altered by FAK inhibitor treatment, immunoblotting analyses were performed on lysates of sensitive (HEY, OVCAR8) and resistant (OVCAR10, SKOV3-IP) cells

Published OnlineFirst June 4, 2014; DOI: 10.1158/1535-7163.MCT-13-1063

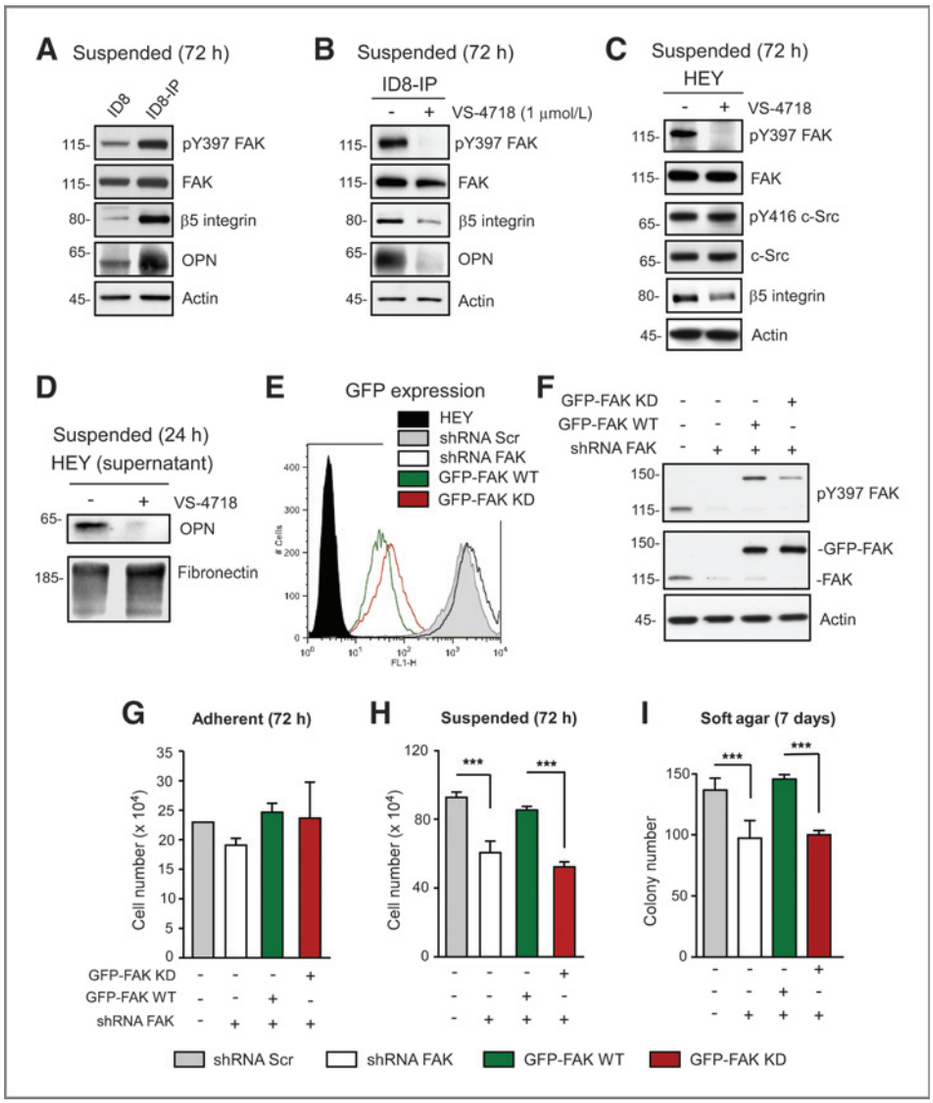

Figure 3. FAK inhibition reduces β5 integrin and osteopontin (OPN) levels in ID8-IP and HEY cells. A, lysates of ID8 and ID8-IP cells grown in suspension for 72 hours immunoblotted for pY397 FAK, total FAK, β5 integrin, osteopontin, and actin. B, lysates of DMSO- or VS-4718–treated ID8-IP cells grown in suspension for 72 hours immunoblotted for pY397 FAK, total FAK, β5 integrin, osteopontin, and actin. C, DMSO- or VS-4718–treated HEY cells in suspension for 72 hours were immunoblotted for pY397 FAK, FAK, Src pY416, c-Src, β5 integrin, osteopontin, and actin. D, conditioned media from anchorage-independent 24-hour DMSO- or VS-4718–treated HEY cells were immunoblotted for osteopontin and fibronectin. E, stable lentiviral scrambled (Scr, gray) or FAK shRNA (white) knockdown HEY cells were transduced to express GFP, GFP-FAK-WT (green), or GFP-FAK KD (red) and analyzed by flow cytometry. Black histogram, parental HEY background fluorescence. F, HEY cells knocked down and reconstituted with FAK were immunoblotted for exogenous GFP-FAK (~150 kDa) and endogenous FAK (~115 kDa) pY397 FAK and total FAK. Actin is a loading control. G–I, growth of Scr shRNA (gray), FAK shRNA, (white), GFP-FAK WT- (green), and GFP-FAK KD-reconstituted (red) HEY cells in adherent (G), suspended (H), and soft agar (I) growth conditions at 72 hours. Values are means (±SD) of triplicate points (***, $P < 0.001$) from at least 2 independent experiments.

grown in suspension for 72 hours in the presence or absence of 1 μmol/L VS-4718 (Fig. 2B). VS-4718 prevented FAK Y397 phosphorylation in SKOV3-IP, HEY, and OVCAR8 cells, whereas FAK Y397 phosphorylation was already low in OVCAR10 cells. Resistant OVCAR10 and SKOV3-IP cells had high Akt S473 phosphorylation and no changes in β5 integrin levels upon VS-4718 addition (Fig. 2B). In contrast, Akt S473 phosphorylation was not detected and β5 integrin levels were decreased in VS-4718–treated sensitive HEY and OVCAR8 cells, compared with controls. These results suggest that FAK inhibitor–resistant cells may contain genetic alterations promoting Akt S473 phosphorylation and that FAK activation may be part of a signaling loop controlling β5 integrin levels in sensitive cells.

FAK activity regulates β5 integrin expression and anchorage-independent cell growth

Intraperitoneal (IP) growth of murine ID8 ovarian carcinoma cells followed by *in vitro* culture resulted in the isolation of aggressive cells, named ID8-IP (12). Compared with parental ID8 cells, FAK Y397 phosphorylation (pY397 FAK), β5 integrin, and osteopontin levels are elevated in ID8-IP cells under anchorage-independent conditions (Fig. 3A). In both ID8-IP and HEY cells, 1 μmol/L VS-4718 treatment selectively lowers pY397 FAK, β5 integrin, and osteopontin levels (Fig. 3B–D). To confirm that this was due to FAK inactivation, HEY cells were transduced with scrambled (Scr) or FAK shRNA to knockdown FAK expression about 90% (Fig. 3E). GFP-tagged FAK-WT or -KD were stably re-expressed in HEY FAK shRNA cells at equivalent levels (Fig. 3E and F). GFP-FAK-WT cells exhibited elevated pY397 FAK compared with GFP-FAK-KD cells (Fig. 3F).

To determine whether loss of FAK expression or activity altered HEY cell growth, analyses were performed under adherent, suspended, and soft agar conditions (Fig. 3G–I). No growth differences were noted when cells were grown on plastic (Fig. 3G), but FAK knockdown reduced

Published OnlineFirst June 4, 2014; DOI: 10.1158/1535-7163.MCT-13-1063

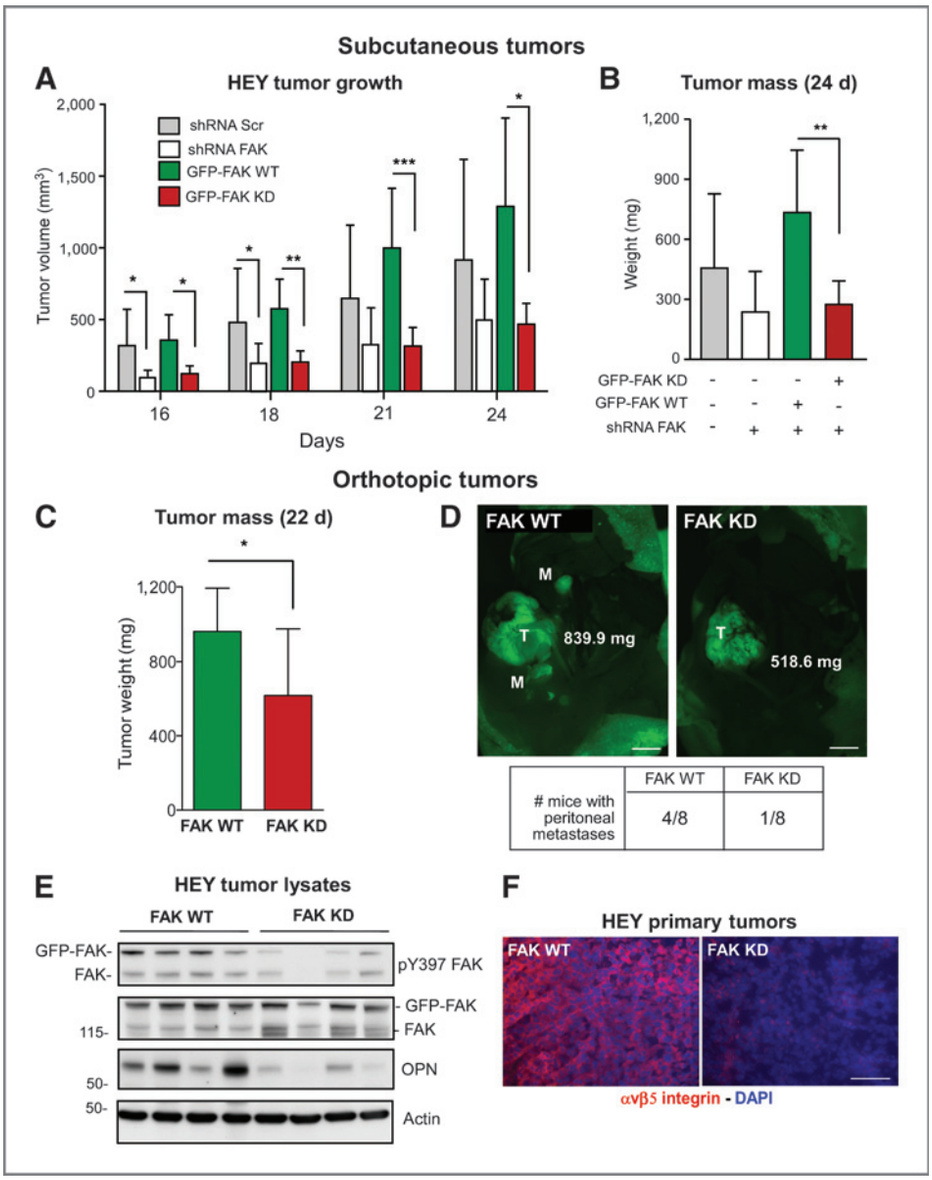

Figure 4. Genetic FAK inhibition prevents HEY tumor growth associated with decreased osteopontin (OPN) and β5 integrin levels. A, mean subcutaneous tumor volume of Scr shRNA (gray, $n = 6$), FAK shRNA (white, $n = 6$), GFP-FAK WT- (green, $n = 5$), and GFP-FAK KD-reconstituted (red, $n = 6$) HEY cells at day 16 to 24 (±SD; *, $P < 0.05$; **, $P < 0.01$; ***, $P < 0.0001$). B, final mean subcutaneous tumor mass in A (±SD; **, $P < 0.01$). C, mean GFP-FAK WT (green, $n = 8$) and GFP-FAK KD (red, $n = 8$) HEY orthotopic tumor mass (±SD; *, $P < 0.05$). D, representative orthotopic tumors (T) and peritoneal metastasis sites (M) as determined by GFP fluorescent imaging. Scale, 0.5 cm. E, lysates from four GFP-FAK WT or four GFP-FAK KD HEY orthotopic tumors analyzed by pY397 FAK, total FAK, osteopontin, and actin immunoblotting. F, fluorescent microscopic images of GFP-FAK WT and GFP-FAK-KD HEY tumor sections stained for αvβ5 integrin (red) and cell nuclei (blue). Scale, 100 μm.

growth in suspension and soft agar (Fig. 3H and I). This was rescued by GFP-FAK-WT but not GFP-FAK-KD re-expression. Correspondingly, FAK knockdown reduced HEY growth as subcutaneous tumors and this was rescued by GFP-FAK-WT but not GFP-FAK-KD re-expression (Fig. 4A and B). GFP-FAK WT also promoted orthotopic HEY tumor growth and spontaneous peritoneal metastasis that was significantly reduced in HEY cells expressing GFP-FAK-KD (Fig. 4C and D). These results show that FAK activity is important for anchorage-independent and ovarian tumor growth.

Analyses of HEY tumors showed reduced pY397 FAK, osteopontin, and αvβ5 integrin levels in GFP-FAK-KD compared with GFP-FAK-WT tumors (Fig. 4E and F). Immunoblotting ID8-IP tumor lysates showed that oral FAK inhibitor administration reduced pY397 FAK, osteopontin, and β5 integrin levels compared with vehicle control-treated mice (Supplementary Fig. S3). Interestingly, qPCR revealed no changes in β5 integrin mRNA levels upon genetic or pharmacological FAK inhibition in HEY cells (Supplementary Fig. S4). Together, these results show that the inhibition of FAK activity in HEY cells decreases tumor growth with a corresponding reduction in β5 integrin protein levels that occurs independently of changes in β5 integrin mRNA expression.

β5 integrin promotes HEY ovarian tumor growth

To determine whether FAK and β5 integrin comprise a signaling axis promoting ovarian tumor growth, 2 independent lentiviral shRNAs were used to stably knockdown HEY β5 integrin expression (Fig. 5A). Flow cytometric analyses showed that αvβ5 integrin was reduced about

Published OnlineFirst June 4, 2014; DOI: 10.1158/1535-7163.MCT-13-1063

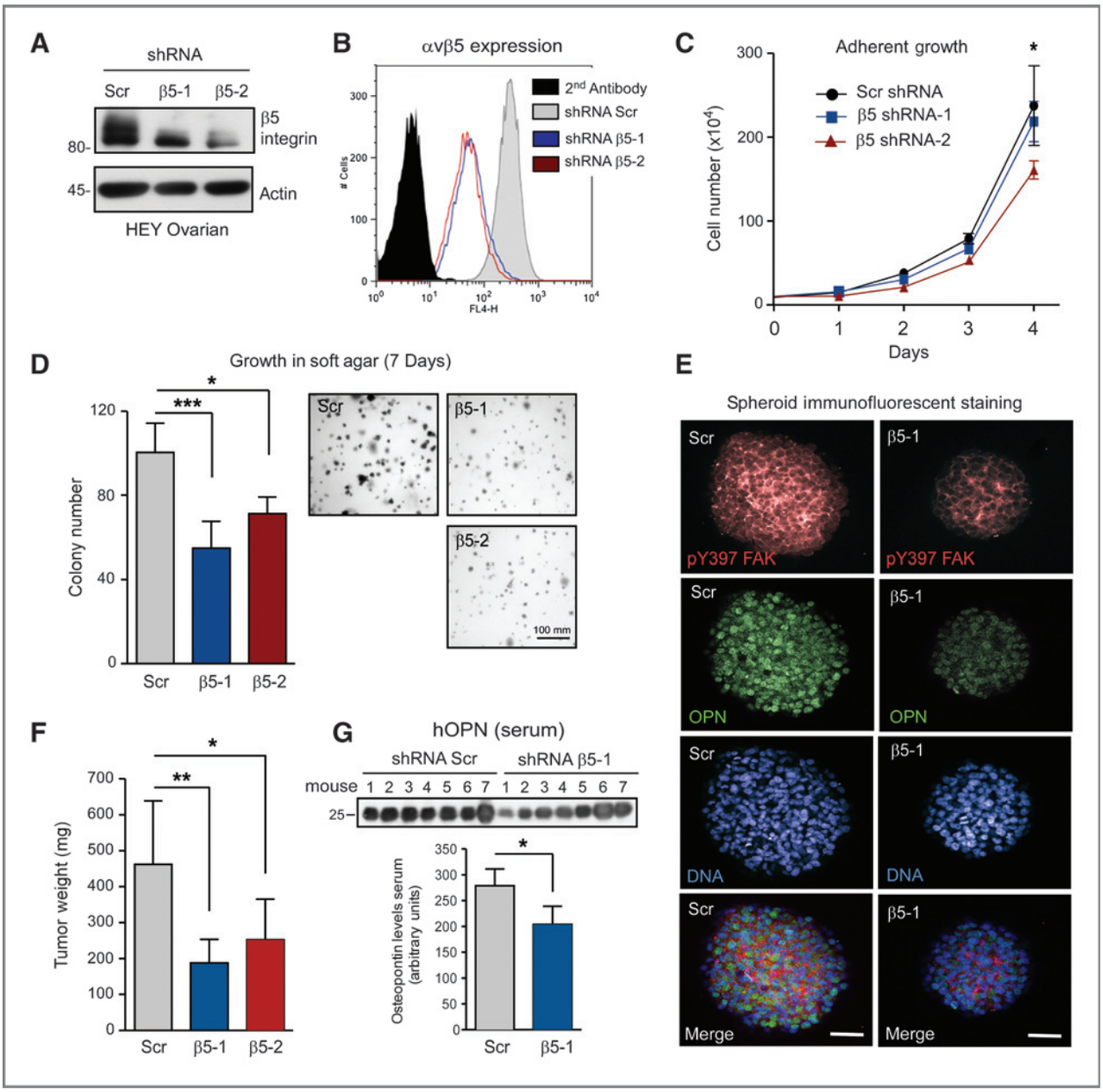

Figure 5. HEY β5 integrin knockdown impairs soft agar and tumor growth with reduced FAK Y397 phosphorylation in spheroids. A, stable HEY β5 integrin knockdown by lentiviral shRNAs (β5-1 and β5-2) as determined by immunoblotting with actin as a loading control. B, flow cytometry of cell surface αvβ5 levels in Scr, β5-1, and β5-2 HEY cells. Black histogram is secondary antibody only. C, mean adherent HEY growth over 4 days (± SD; *, $P < 0.05$). D, mean Scr, β5-1, and β5-2 HEY soft agar colony growth over 7 days (± SD; *, $P < 0.05$; ***, $P < 0.001$). E, representative spheroid fluorescent staining for pY397 FAK (red), osteopontin (green), and cell nuclei (blue) of Scr and β5-1 shRNA HEY cells. Scale, 50 μm. F, orthotopic tumor growth of Scr ($n = 7$), β5-1 ($n = 9$), and β5-2 ($n = 10$) HEY cells in the ovarian bursa. Values are mean tumor mass after 21 days (± SD; *, $P < 0.05$; **, $P < 0.01$). G, serum from Scr and β5-1 HEY tumor–bearing mice was analyzed by anti-hOPN immunoblotting. Densitometry was used to determine mean values ($n = 7$ tumors each, ±SD; *, $P < 0.05$).

10-fold on the surface of HEY cells (Fig. 5B). HEY β5 integrin knockdown did not result in compensatory increases in αvβ3 or β1 integrin surface expression (Supplementary Fig. S5). β5 knockdown minimally affected the growth of HEY cells in adherent conditions compared with the scrambled control (Fig. 5C). In contrast, β5 knockdown significantly reduced HEY growth in soft agar (Fig. 5D). This was associated with decreased FAK Y397 phosphorylation and osteopontin expression as determined by immunofluorescent staining of spheroids (Fig. 5E). When injected orthotopically into the ovarian bursa space, HEY β5 integrin knockdown cells resulted in decreased tumor size after 21 days and reduced serum levels of cleaved (25 kDa) human osteopontin (Fig. 5F and G). Together, these

Published OnlineFirst June 4, 2014; DOI: 10.1158/1535-7163.MCT-13-1063

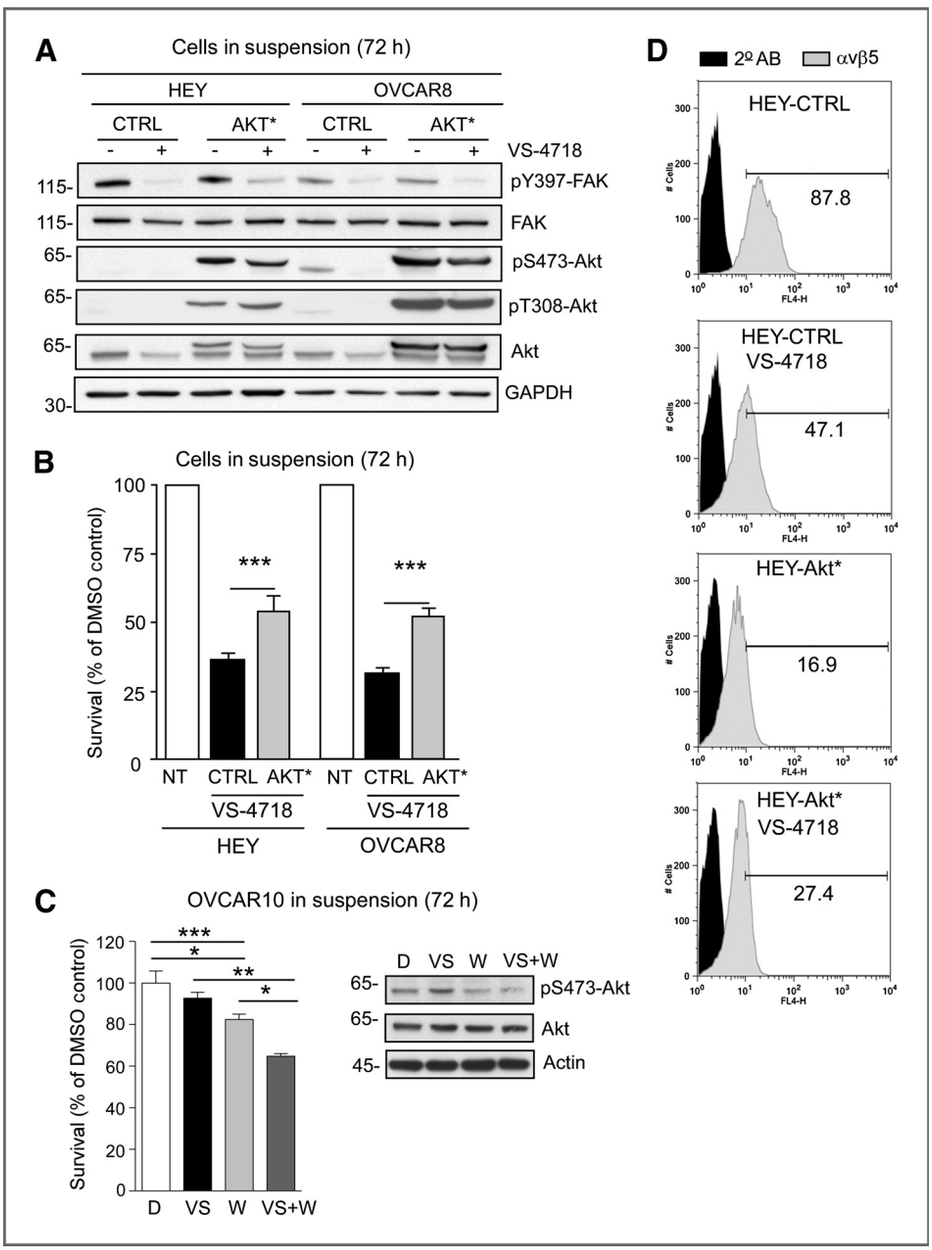

Figure 6. Stable activated Akt (Akt*) expression in HEY and OVCAR8 cells promotes anchorage-independent growth and β5 integrin surface expression in the presence of VS-4718. A, immunoblotting for pY397 FAK, FAK, pS473 Akt, pT308 Akt, Akt, and GAPDH in control vector (CTRL) or Akt*-expressing HEY or OVCAR8 cells cultured in suspension for 72 hours with 1 μmol/L VS-4718 as indicated. B, HEY and OVCAR8 nontransfected (NT), CTRL-, and Akt*-expressing cells were evaluated for anchorage-independent growth over 72 hours in DMSO or 1 μmol/L VS-4718. C, OVCAR10 cells plated in suspension for 72 hours and treated with DMSO (D), 0.1 μmol/L VS-4718 (VS), or 0.1 μmol/L wortmannin (W) alone or in combination. Right, immunoblotting for pS473 Akt, Akt, and actin. B and C, values are means (±SEM) of triplicate points from 3 independent experiments (*, $P < 0.05$; **, $P < 0.01$; ***, $P < 0.001$). D, flow cytometry of αvβ5 surface expression in CTRL or Akt* HEY cells cultured in DMSO or 1 μmol/L VS-4718 for 72 hours. Dark histogram is secondary antibody only.

results show that the FAK–β5 integrin signaling axis promotes HEY tumor growth and that osteopontin may serve as a secreted ligand in this pathway.

Partial phenotypic rescue by activated Akt expression

FAK inhibitor–resistant SKOV3-IP and OVCAR10 cells exhibited elevated Akt S473 phosphorylation, an indirect marker of Akt activation in anchorage-independent conditions (Fig. 2B). One possible explanation is that SKOV3-IP cells contain activating mutations in *PIK3CA* (Supplementary Table S2) and this may bypass effects of upstream FAK inhibition. Moreover, studies have shown that inhibition of mTOR, a downstream target of Akt, prevents SKOV3 and OVCAR10 cell growth (34). To determine whether Akt activation is sufficient to bypass FAK inhibition, membrane-targeted myristoylated Akt (Akt*) was stably expressed in sensitive HEY and OVCAR8 cells (Fig. 6). Immunoblotting of lysates showed that Akt* remained highly phosphorylated at S473 and T308 in the presence of 1 μmol/L VS-4718 treatment of cells for 72 hours in suspension (Fig. 6A). Although Akt* remained active, FAK Y397 phosphorylation was equally reduced by VS-4718 addition in control vector (CTRL) and Akt*-expressing HEY and OVCAR8 cells (Fig. 6A). These results are consistent with Akt being downstream of FAK.

Published OnlineFirst June 4, 2014; DOI: 10.1158/1535-7163.MCT-13-1063

To test the effects of Akt* on suspended cell growth, CTRL and Akt*-expressing HEY and OVCAR8 cells were grown in suspension in the presence or absence of 1 μmol/L VS-4718 treatment for 72 hours (Fig. 6B). CTRL HEY and OVCAR8 cells remained highly sensitive to FAK inhibitor addition (70% growth inhibition), and surprisingly, Akt*-expressing cells showed about 50% growth inhibition to VS-4718. Although this was significantly higher than CTRL cells, Akt* did not completely suppress HEY and OVCAR8 sensitivity to VS-4718 growth inhibition (Fig. 6B). When resistant OVCAR10 cells were treated with VS-4718 in combination with wortmannin (a PI3K inhibitor), anchorage-independent growth and Akt S473 phosphorylation were decreased (Fig. 6C). Finally, when analyzing β5 integrin surface expression, there was a significant reduction in CTRL HEY cells upon VS-4718 addition and this reduction was not observed in HEY Akt* cells (Fig. 6D). These results support the conclusion that FAK to Akt signaling is important for maintenance of β5 integrin surface expression. However, ovarian tumor growth resistance to FAK inhibitor treatment likely involves multiple pathways in addition to Akt activation.

Discussion

The high mortality rate in ovarian cancer is partially due to its unusual mechanism of dissemination. Cells are shed from the primary tumor into the peritoneal cavity where tumor growth occurs in an anchorage-independent manner as clumps of aggregated cells termed spheroids (2). Under these conditions, interactions between integrins and matrix proteins promote cell survival and proliferation. We find that pharmacologic and genetic inhibition of FAK decreases ovarian carcinoma β5 integrin and osteopontin levels in tumors. This role for FAK activity is distinct from the canonical linkage of matrix–integrin binding leading to FAK activation (32). FAK inhibition or β5 knockdown reduced ovarian tumor cell growth under anchorage-independent conditions with corresponding decreases in orthotopic tumor growth. High osteopontin, β5 integrin, and FAK mRNA levels are associated with decreased survival of patients with serous ovarian cancer and IHC analyses confirmed that protein levels correlate with increasing serous ovarian tumor stage. Our results support a model whereby FAK inhibition disrupts autocrine or paracrine signaling regulating β5 integrin and osteopontin levels in ovarian carcinoma cells. β5 integrin expression may serve as a biomarker for serous ovarian carcinoma cells that possess active FAK signaling. Moreover, reduction of β5 integrin levels may serve as an indicator of FAK inhibitor effectiveness in ovarian cancer.

Notably, genetic and pharmacological FAK inhibition prevented anchorage-independent but not adherent ovarian cancer cell growth. Moreover, we identified cells as either sensitive (HEY, OVCAR8) or resistant (SKOV3-IP, OVCAR10) to VS-4718 treatment. Despite the fact that several drugs have low efficacy on tumor cells cultured as spheroids (35, 36), nanomolar concentrations of VS-4718 prevented sensitive ovarian cancer cell growth as spheroids by triggering cell-cycle blockage and apoptosis. As FAK inhibitors are being tested in clinical trials, it is important to identify molecular drivers of potential resistance as a means to select patients that may preferentially benefit from FAK inhibitor treatment.

Analysis of mutation frequency, copy number, or gene expression changes revealed that about 45% of serous ovarian cancer contain some type of alteration that would activate *PI3K* and *RAS* signaling pathways (37). Interestingly, studies have found that pharmacologic FAK inhibition (PF-271, 40 mg/kg) decreased tumor volume in a *KRAS* G12D mouse model of non–small cell lung carcinoma and human lung tumor cell xenografts (38). In addition, VS-4718 (PND-1186) FAK inhibition was effective in preventing MDA-MB-231 (*KRAS* G13D and *BRAF* G464V) breast carcinoma orthotopic tumor growth and metastasis (18). Sequencing of the HEY-A8 ovarian tumor subclone reveals *KRAS* G12D and *BRAF* G464E activating mutations (Supplementary Table S2; ref. 39), and HEY-A8 cells are responsive to pharmacologic FAK inhibition (Verastem, VS-6063; ref. 31). Because HEY cells are sensitive to VS-4718 FAK inhibition, these studies support the notion that *KRAS* and *BRAF* oncogenic mutations do not confer a FAK inhibitor–resistant phenotype.

Furthermore, it is known that PI3K and Akt activation can be downstream targets of FAK signaling in ovarian cancer (31, 32). Sequencing of SKOV3 and IGROV1 ovarian tumor cells has revealed activating mutations in *PIK3CA* (Supplementary Table S2; ref. 39). Although combined PI3K and FAK inhibition had additive effects in preventing OVCAR10 anchorage-independent growth, expression of activated Akt was not sufficient to generate a FAK inhibitor–resistant phenotype in HEY or OVCAR8 cells. Together, these results support the notion that FAK signaling impacts a growth-promoting pathway distinct from that activated by oncogenic mutations in *KRAS, BRAF, and PIK3CA.*

Disclosure of Potential Conflicts of Interest

No potential conflicts of interest were disclosed.

Authors' Contributions

Conception and design: I. Tancioni, D.D. Schlaepfer
Development of methodology: I. Tancioni, D.D. Schlaepfer
Acquisition of data (provided animals, acquired and managed patients, provided facilities, etc.): I. Tancioni, S. Uryu, F.J. Sulzmaier, N.R. Shah, C. Lawson, N.L.G. Miller, C. Jean, X.L. Chen, K.K. Ward
Analysis and interpretation of data (e.g., statistical analysis, biostatistics, computational analysis): I. Tancioni, F.J. Sulzmaier, N.R. Shah, C. Lawson, N.L.G. Miller, C. Jean, K.K. Ward, D.D. Schlaepfer
Writing, review, and or revision of the manuscript: I. Tancioni, F.J. Sulzmaier, N.R. Shah, C. Lawson, N.L.G. Miller, C. Jean, K.K. Ward, D.D. Schlaepfer
Administrative, technical, or material support (i.e., reporting or organizing data, constructing databases): S. Uryu, N.L.G. Miller, X.L. Chen
Study supervision: I. Tancioni, D.D. Schlaepfer

Published OnlineFirst June 4, 2014; DOI: 10.1158/1535-7163.MCT-13-1063

Acknowledgments

The authors thank David Tarin for providing guidance and expertise in tumor pathology.

Grant Support

This work was supported by NIH grant CA102310 and a grant from "Nine Girls Ask?" to D.D. Schlaepfer. I. Tancioni was supported by a grant from Susan G. Komen for the Cure (KG111237). F.J. Sulzmaier was supported by NIH training grant (T32-CA121938). C. Lawson was supported in part by an Ovarian Cancer Research Fund fellowship (258835). C. Jean was supported by an American Heart Association fellowship (12POST11760014). N.L.G. Miller was supported by a National Research Service Award (1F32CA159558). N.R. Shah and K.K. Ward are fellows of the UCSD Reproductive Medicine Gynecologic Oncology program.

The costs of publication of this article were defrayed in part by the payment of page charges. This article must therefore be hereby marked *advertisement* in accordance with 18 U.S.C. Section 1734 solely to indicate this fact.

Received January 8, 2014; revised May 5, 2014; accepted May 19, 2014; published OnlineFirst June 4, 2014.

References

1. Siegel R, Ma J, Zou Z, Jemal A. Cancer statistics, 2014. CA: A Cancer J Clin 2014;64:9–29.
2. Shield K, Ackland ML, Ahmed N, Rice GE. Multicellular spheroids in ovarian cancer metastases: Biology and pathology. Gynecol Oncol 2009;113:143–8.
3. Hanahan D, Weinberg RA. Hallmarks of cancer: the next generation. Cell 2011;144:646–74.
4. Kipps E, Tan DS, Kaye SB. Meeting the challenge of ascites in ovarian cancer: new avenues for therapy and research. Nat Rev Cancer 2013;13:273–82.
5. Carduner L, Agniel R, Kellouche S, Picot CR, Blanc-Fournier C, Leroy-Dudal J, et al. Ovarian cancer ascites-derived vitronectin and fibronectin: combined purification, molecular features and effects on cell response. Biochim Biophys Acta 2013;1830:4885–97.
6. Kim JH, Skates SJ, Uede T, Wong KK, Schorge JO, Feltmate CM, et al. Osteopontin as a potential diagnostic biomarker for ovarian cancer. JAMA 2002;287:1671–9.
7. Visintin I, Feng Z, Longton G, Ward DC, Alvero AB, Lai Y, et al. Diagnostic markers for early detection of ovarian cancer. Clin Cancer Res 2008;14:1065–72.
8. Casey RC, Burleson KM, Skubitz KM, Pambuccian SE, Oegema TR Jr, Ruff LE, et al. Beta 1-integrins regulate the formation and adhesion of ovarian carcinoma multicellular spheroids. Am J Pathol 2001;159:2071–80.
9. Iwanicki MP, Davidowitz RA, Ng MR, Besser A, Muranen T, Merritt M, et al. Ovarian cancer spheroids use myosin-generated force to clear the mesothelium. Cancer Discov 2011;1:144–57.
10. Mitra AK, Sawada K, Tiwari P, Mui K, Gwin K, Lengyel E. Ligand-independent activation of c-Met by fibronectin and alpha(5)beta(1)-integrin regulates ovarian cancer invasion and metastasis. Oncogene 2011;30:1566–76.
11. Bell-McGuinn KM, Matthews CM, Ho SN, Barve M, Gilbert L, Penson RT, et al. A phase II, single-arm study of the anti-alpha5beta1 integrin antibody volociximab as monotherapy in patients with platinum-resistant advanced epithelial ovarian or primary peritoneal cancer. Gynecol Oncol 2011;121:273–9.
12. Ward KK, Tancioni I, Lawson C, Miller NL, Jean C, Chen XL, et al. Inhibition of focal adhesion kinase (FAK) activity prevents anchorage-independent ovarian carcinoma cell growth and tumor progression. Clin Exp Metastasis 2013;30:579–94.
13. Desgrosellier JS, Cheresh DA. Integrins in cancer: biological implications and therapeutic opportunities. Nat Rev Cancer 2010;10:9–22.
14. Slack-Davis JK, Martin KH, Tilghman RW, Iwanicki M, Ung EJ, Autry C, et al. Cellular characterization of a novel focal adhesion kinase inhibitor. J Biol Chem 2007;282:14845–52.
15. Lim ST, Chen XL, Tomar A, Miller NL, Yoo J, Schlaepfer DD. Knock-in mutation reveals an essential role for focal adhesion kinase activity in blood vessel morphogenesis and cell motility-polarity but not cell proliferation. J Biol Chem 2010;285:21526–36.
16. Halder J, Lin YG, Merritt WM, Spannuth WA, Nick AM, Honda T, et al. Therapeutic efficacy of a novel focal adhesion kinase inhibitor TAE226 in ovarian carcinoma. Cancer Res 2007;67:10976–83.
17. Roberts WG, Ung E, Whalen P, Cooper B, Hulford C, Autry C, et al. Antitumor activity and pharmacology of a selective focal adhesion kinase inhibitor, PF-562,271. Cancer Res 2008;68:1935–44.
18. Walsh C, Tanjoni I, Uryu S, Tomar A, Nam JO, Luo H, et al. Oral delivery of PND-1186 FAK inhibitor decreases tumor growth and spontaneous breast to lung metastasis in pre-clinical models. Cancer Biol Ther 2010;9:778–90.
19. Tanjoni I, Walsh C, Uryu S, Tomar A, Nam JO, Mielgo A, et al. PND-1186 FAK inhibitor selectively promotes tumor cell apoptosis in three-dimensional environments. Cancer Biol Ther 2010;9:764–77.
20. Infante JR, Camidge DR, Mileshkin LR, Chen EX, Hicks RJ, Rischin D, et al. Safety, pharmacokinetic, and pharmacodynamic phase I dose-escalation trial of PF-00562271, an inhibitor of focal adhesion kinase, in advanced solid tumors. J Clin Oncol 2012;30:1527–33.
21. Heinrich T, Seenisamy J, Emmanuvel L, Kulkarni SS, Bomke J, Rohdich F, et al. Fragment-based discovery of new highly substituted 1H-pyrrolo[2,3-b]- and 3H-imidazolo[4,5-b]-pyridines as focal adhesion kinase inhibitors. J Med Chem 2013;56:1160–70.
22. Yu D, Wolf JK, Scanlon M, Price JE, Hung MC. Enhanced c-erbB-2/neu expression in human ovarian cancer cells correlates with more severe malignancy that can be suppressed by E1A. Cancer Res 1993;53:891–8.
23. Lim ST, Chen XL, Lim Y, Hanson DA, Vo TT, Howerton K, et al. Nuclear FAK promotes cell proliferation and survival through FERM-enhanced p53 degradation. Mol Cell 2008;29:9–22.
24. Weiswald LB, Guinebretiere JM, Richon S, Bellet D, Saubamea B, Dangles-Marie V. In situ protein expression in tumour spheres: development of an immunostaining protocol for confocal microscopy. BMC Cancer 2010;10:106.
25. Gyorffy B, Lanczky A, Szallasi Z. Implementing an online tool for genome-wide validation of survival-associated biomarkers in ovarian-cancer using microarray data from 1287 patients. Endocr Relat Cancer 2012;19:197–208.
26. Davidson B, Goldberg I, Reich R, Tell L, Dong HP, Trope CG, et al. AlphaV- and beta1-integrin subunits are commonly expressed in malignant effusions from ovarian carcinoma patients. Gynecol Oncol 2003;90:248–57.
27. Kaur S, Kenny HA, Jagadeeswaran S, Zillhardt MR, Montag AG, Kistner E, et al. {beta}3-integrin expression on tumor cells inhibits tumor progression, reduces metastasis, and is associated with a favorable prognosis in patients with ovarian cancer. Am J Pathol 2009;175:2184–96.
28. Spentzos D, Levine DA, Ramoni MF, Joseph M, Gu X, Boyd J, et al. Gene expression signature with independent prognostic significance in epithelial ovarian cancer. J Clin Oncol 2004;22:4700–10.
29. Grisaru-Granovsky S, Salah Z, Maoz M, Pruss D, Beller U, Bar-Shavit R. Differential expression of protease activated receptor 1 (Par1) and pY397FAK in benign and malignant human ovarian tissue samples. Int J Cancer 2005;113:372–8.
30. Sood AK, Coffin JE, Schneider GB, Fletcher MS, DeYoung BR, Gruman LM, et al. Biological significance of focal adhesion kinase in ovarian cancer: role in migration and invasion. Am J Pathol 2004;165:1087–95.
31. Kang Y, Hu W, Ivan C, Dalton HJ, Miyake T, Pecot CV, et al. Role of focal adhesion kinase in regulating YB-1-mediated paclitaxel resistance in ovarian cancer. J Natl Cancer Inst 2013;105:1485–95.
32. Lane D, Goncharenko-Khaider N, Rancourt C, Piche A. Ovarian cancer ascites protects from TRAIL-induced cell death through alphavbeta5 integrin-mediated focal adhesion kinase and Akt activation. Oncogene 2010;29:3519–31.

Published OnlineFirst June 4, 2014; DOI: 10.1158/1535-7163.MCT-13-1063

33. Altomare DA, Wang HQ, Skele KL, De Rienzo A, Klein-Szanto AJ, Godwin AK, et al. AKT and mTOR phosphorylation is frequently detected in ovarian cancer and can be targeted to disrupt ovarian tumor cell growth. Oncogene 2004;23:5853–7.

34. Mabuchi S, Altomare DA, Connolly DC, Klein-Szanto A, Litwin S, Hoelzle MK, et al. RAD001 (Everolimus) delays tumor onset and progression in a transgenic mouse model of ovarian cancer. Cancer Res 2007;67:2408–13.

35. Friedrich J, Ebner R, Kunz-Schughart LA. Experimental anti-tumor therapy in 3-D: spheroids–old hat or new challenge? Int J Radiat Biol 2007;83:849–71.

36. Friedrich J, Seidel C, Ebner R, Kunz-Schughart LA. Spheroid-based drug screen: considerations and practical approach. Nat Protoc 2009;4:309–24.

37. Cancer Genome Atlas Research N. Integrated genomic analyses of ovarian carcinoma. Nature 2011;474:609–15.

38. Konstantinidou G, Ramadori G, Torti F, Kangasniemi K, Ramirez RE, Cai Y, et al. RHOA-FAK is a required signaling axis for the maintenance of KRAS-driven lung adenocarcinomas. Cancer Discov 2013;3:444–57.

39. Domcke S, Sinha R, Levine DA, Sander C, Schultz N. Evaluating cell lines as tumour models by comparison of genomic profiles. Nat Commun 2013;4:2126.

FAK inhibition disrupts a β5 integrin signaling axis controlling anchorage-independent ovarian carcinoma growth

Isabelle Tancioni, Sean Uryu, Florian J. Sulzmaier, Nina R. Shah, Christine Lawson, Nichol L.G. Miller, Christine Jean, Xiao Lei Chen, Kristy K. Ward, and David D. Schlaepfer[1]

Department of Reproductive Medicine, UCSD Moores Cancer Center, La Jolla, CA 92093

Supplementary Material and Methods

Cell cycle and apoptosis analyses

For cell cycle analyses, cells were collected as a single cell suspension by limited trypsin treatment and fixed in 70% ethanol. Cells were incubated in 100 µl of PBS containing DNAse-free RNAse (100 µg/ml, Qiagen) and after 45 min, propidium iodide (PI) (5 µg/ml) was added prior to flow cytometry. For cell apoptosis analyses, cells were stained using APC-conjugated annexin V and 7-amino-actinomycin (7-AAD) (BD Pharmingen), and analyzed within 1 h by flow cytometry.

Real-Time quantitative PCR analyses

RNA was extracted from FAK WT, FAK KD, DMSO- and VS-4718-treated HEY cells using the RNeasy Kit (Qiagen). β5 integrin and actin (used as normalization control) were amplified with specific primers (Supplementary Table 1). 480 SYBR green master mix (BioPioneer) with a LighterCycler 480 (Roche) was used for PCR. Cycle conditions were 40 cycles of 94C for 15 s, 55C for 30 s, and 72C for 30 seconds. The normalized mRNA level was defined as DCt = (target gene)-Ct (reference gene) and presented as fold difference between control and test samples (DCt control-DCt test).

Supplemental Table 1. Antibodies, DNA plasmids, and probe sets used in this study.

Antibody	**Usage**	**Clone-Number**	**Company**
c-Src	IB	SC-18	Santa Cruz Biotechnology
GAPDH	IB	clone 374	Millipore
FAK	IB	clone 4.47	Millipore
pY397 FAK	IB	141-9	Life Technologies
pY397 FAK	IHC	AB4803	Abcam
osteopontin	IHC-paraffin	clone 10A16	IBL International
β5 integrin	IB	AB15459	Abcam
pY416 c-Src	IB	2101	Cell Signaling Technologies
osteopontin	IB	AF1433	R&D Systems
osteopontin	IB	AF808	R&D Systems
osteopontin	IB	clone LFMB-14	Santa Cruz Biotechnology
pS473 AKT	IB	9271	Cell Signaling Technologies
pT308 AKT	IB	C31E5E	Cell Signaling Technologies
AKT	IB	C67E7	Cell Signaling Technologies
fibronectin	IB	610077	BD Biosciences
β-actin	IB	AC-74	Sigma
Goat anti-rabbit Alexa Fluor-647	IF	A21235	Life Technologies
Goat anti-mouse Alexa Fluor-488	IF	A11001	Life Technologies
Biotinylated goat anti-rabbit IgG	IHC-paraffin	BA-1000	Vector Laboratories
Biotinylated rabbit anti-goat IgG	IHC-paraffin	BA-5000	Vector Laboratories
Biotinylated goat anti-mouse IgG	IHC-paraffin	BA-9200	Vector Laboratories
Goat anti-mouse IgG APC	Flow	BD 550826	BD Biosciences
Goat anti-rat IgG APC	Flow	17-4822	eBioscience
β1 integrin	Flow	TDM29	Millipore
β3 integrin	Flow	SAP	Millipore
αvβ5 integrin	Flow	clone P1F6	Millipore
Plasmid		**Reference**	**Company**
shRNA β5-1		002213.3-1225s1c1	Mission-Sigma
shRNA β5-2		002213.3-2588s1c1	Mission-Sigma
shRNA Scr		SHC016	Mission-Sigma
pBabe-Puro-Myr-Flag-AKT1		15294	Addgene
pBabe-puro		1764	Addgene
Probe Set	**Affymetrix ID**	**Express Range**	**Cutoff Value (Mean)**
β5 integrin (ITGB5)	201125_s_at	25 - 11900	2935
FAK (PTK2)	208820_at	36 - 9759	1861
osteopontin (OPN)	209875_s_at	23 - 48120	7965
αv integrin (ITGAV)	202351_at	16 - 16831	3611
β1 integrin (ITGB1)	211945_s_at	327 - 24340	9867
β3 integrin (ITGB3)	204627_s_at	1 - 5725	44
RT-PCR-Primers	**Sequence**		**Product size (Bp)**
ITGB5 Forward	AAAATGGCTGTGGAGGTGAG		369
ITGB5 Reverse	GTGCCGTGTAGGAGAAAGGA		
ACTB Forward	GCGAGCACAGACCCTCGCCTTTG		90
ACTB Reverse	ACGACGAGCGCGGCGATATCAT		

Supplemental Table 2. Background information on the breast and ovarian carcinoma cell lines used in this study.

Cells	Source	Culture media	Cancer Type	Selected Genetic Events (http://www.broadinstitute.org/ccle)
BT474	ATCC	(1)	Human breast invasive ductal carcinoma luminal subtype	PIK3CA (K111N) TP53 (E285K)
SKOV3	J. Chien (Rochester)	(2)	Human ovarian adenocarcinoma (subtype not specified) NCI-60	ARID1A (Q586*) PIK3CA (H1047R)
HEY	S. Howell (UCSD)	(2)	Human ovarian serous adenocarcinoma	[Information on HEY-A8 subclone] BRAF (G464E) KRAS (G12D)
OVCAR3	D. Connolly (Fox Chase)	(2)	Human ovarian serous adenocarcinoma refractory to cisplatin NCI-60	TP53 (R248Q)
OVCAR8	D.Connolly (Fox Chase)	(3)	Human ovarian adenocarcinoma (subtype not specified) refractory to carboplatin NCI-60	CTNNB1 (Q26R) ERBB2 (G776V) KRAS (P121H) TP53 (Y126_splice)
OVCAR10	D. Connolly (Fox Chase)	(3)	Human ovarian adenocarcinoma (subtype not specified) refractory to carboplatin	(undetermined)
IGROV1	J. Chien (Rochester)	(2)	Human ovarian adenocarcinoma (subtype not specified) NCI-60	ARID1A (M274*, G1847*) PIK3CA (R38C) PTEN (Y155C, V317*) TP53 (Y126C)
ID8	K. Roby (Kansas)	(2)	high passage murine ovarian surface epithelial cells	(undetermined)

(1) RPMI supplemented with 10% fetal bovine serum (FBS), 0.1 mM non-essential amino acids, 2 mM glutamine, 100 U/ml penicillin, and 100 μg/ml streptomycin.
(2) DMEM supplemented with 10% FBS, 0.1 mM non-essential amino acids, 2 mM glutamine, 100 U/ml penicillin, and 100 μg/ml streptomycin.
(3) RPMI supplemented with 10% FBS, 2 mM glutamine, 0.25 units/mL insulin, 100 U/ml penicillin, and 100 μg/ml streptomycin.

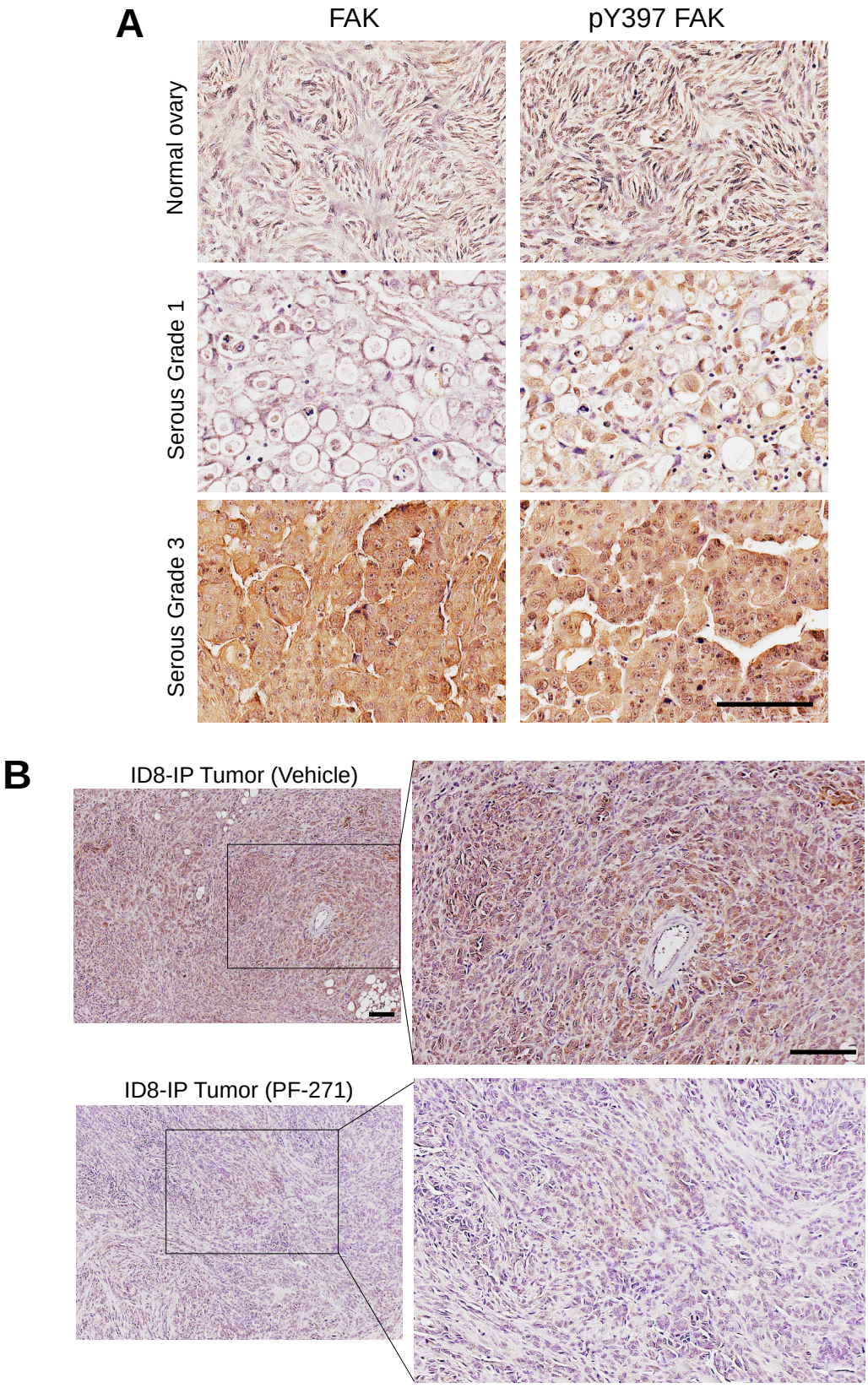

Supplemental Figure 1. FAK and pY397 FAK immunostaining of human tissue array. A, Higher magnification of human tumor tissue array cores stained for FAK and pY397 FAK. B, Pharmacological FAK inhibition reduces the reactivity of anti-pY397 FAK antibody in ID8-IP tumors. B, representative immunohistochemical staining of paraffin-embedded tumors from ID8-IP orthotopic tumors in mice treated with vehicle or PF-271 (30 mg/kg) by oral gavage. Scale is 100 μM.

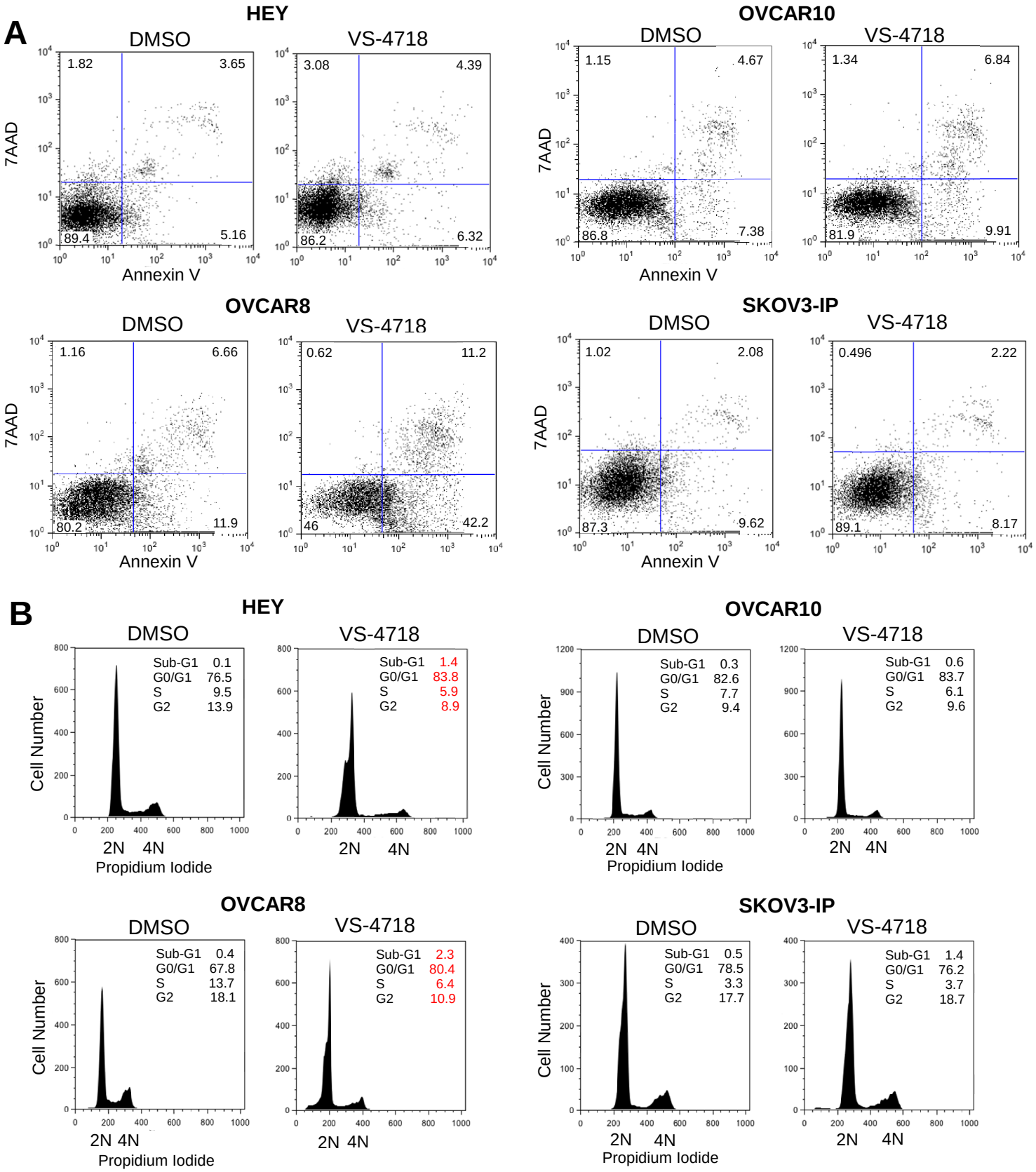

Supplemental Figure 2. Cell survival and cell cycle progression analyses of VS-4718 FAK inhibitor sensitive (HEY and OVCAR8) and resistant (OVCAR10 and SKOV3-IP) cells. Cells were cultured in the presence of DMSO or 1 μM VS-4718 for 72 h in suspension. A, flow cytometry was used to determine the amount of annexin V binding or 7-amino-actinomycin (7-AAD) cell staining. 7-AAD staining of control cells determined viable cell gates. OVCAR8 cells show increased 7-AAD staining after VS-4718 treatment. B, cell cycle analyses as determined by propidium iodide (PI) staining and flow cytometry. Relative DNA content is indicated. Both VS-4718-treated HEY and OVCAR8 cells show decreased S phase, increased GO/G1 and G2 levels, and a sub-G0/G1 shoulder peak compared to controls. No changes were noted between control and VS-4718-treated OVCAR10 and SKOV3-IP cells. Results shown were from a representative experiment that was repeated three independent times.

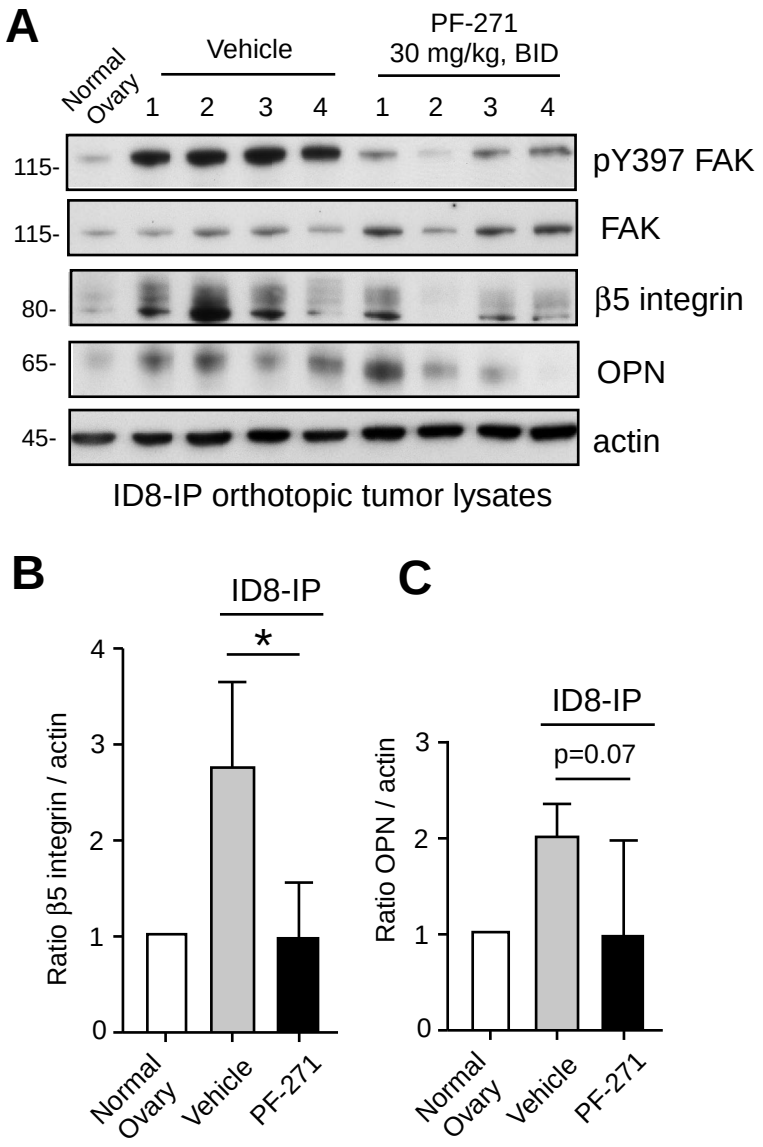

Supplemental Figure 3. Pharmacological FAK inhibition decreases ß5 integrin and osteopontin (OPN) levels in ID8-IP cells *in vivo*. A, protein lysates from normal ovary or ID8-IP orthotopic tumors in mice treated with vehicle (n=4) or PF-271 (30 mg/kg, n=4) by oral gavage as described in [12] were analyzed after 28 days by immunoblotting for pY397 FAK, total FAK, ß5 integrin, OPN, and actin. B, ratio of ß5 integrin to actin. C, ratio of OPN to actin. E and F, values are means (+/- SD, * $p<0.05$) from the indicated ID8-IP tumor samples (n=4) normalized to normal ovary (set to 1) and determined by densitometry using Image J.

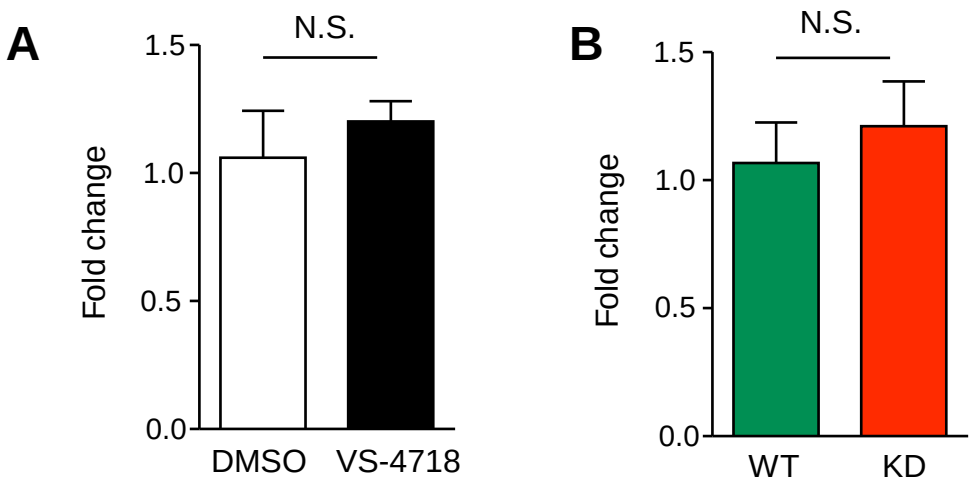

Supplemental Figure 4. qPCR verification of ß5 transcripts. A, qPCR was performed on HEY cells treated for 24 hours with VS-4718 or DMSO. B, qPCR analyses of mRNA levels from ß5 GFP-FAK-WT (WT) and GFP-FAK-KD (KD) HEY cells. Fold change as compared to actin (+/- SD) is shown. Data represent triplicate points from 3 independent experiments. N.S. (not significant difference).

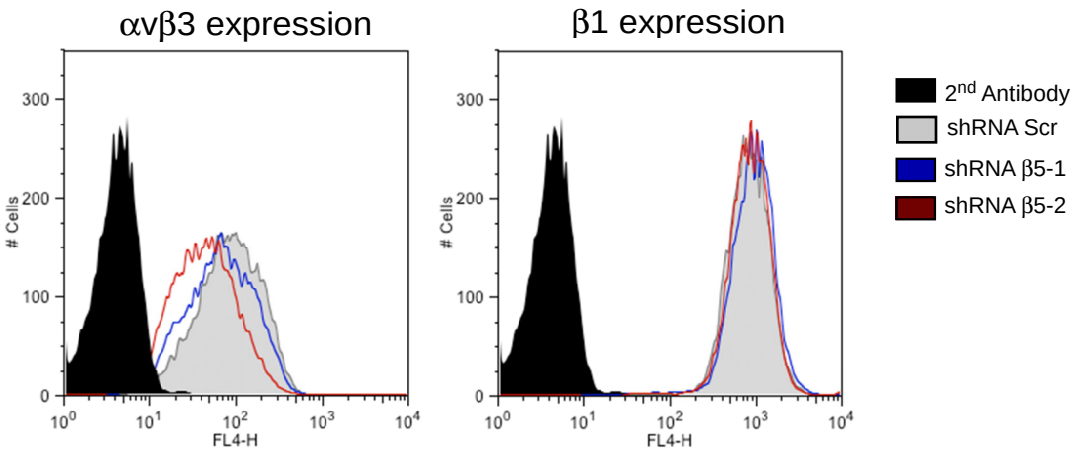

Supplemental Figure 5. Integrin surface expression in HEY ß5 integrin knockdown cells. Flow cytometry of anti-avß3 and anti-ß1 integrin levels. Histograms from Scr (gray), ß5-1 (blue), and ß5-2 (red) HEY cells. Black histogram, parental HEY background fluorescence. Anti-integrin antibodies used are shown in Supplemental Table I.